

UCLA

UCLA Previously Published Works

Title

ImmunoPET of Malignant and Normal B Cells with 89Zr- and 124I-Labeled Obinutuzumab Antibody Fragments Reveals Differential CD20 Internalization In Vivo

Permalink

<https://escholarship.org/uc/item/4013f2kr>

Journal

Clinical Cancer Research, 23(23)

ISSN

1078-0432

Authors

Zettlitz, Kirstin A
Tavaré, Richard
Knowles, Scott M
[et al.](#)

Publication Date

2017-12-01

DOI

10.1158/1078-0432.ccr-17-0855

Peer reviewed



HHS Public Access

Author manuscript

Clin Cancer Res. Author manuscript; available in PMC 2018 December 01.

Published in final edited form as:

Clin Cancer Res. 2017 December 01; 23(23): 7242–7252. doi:10.1158/1078-0432.CCR-17-0855.

ImmunoPET of malignant and normal B cells with ⁸⁹Zr- and ¹²⁴I-labeled obinutuzumab antibody fragments reveals differential CD20 internalization *in vivo*

Kirstin A. Zettlitz¹, Richard Tavaré^{1,3}, Scott M. Knowles^{1,4}, Kristopher K. Steward^{2,5}, John M. Timmerman², and Anna M. Wu¹

¹Crump Institute for Molecular Imaging, Department of Molecular and Medical Pharmacology, David Geffen School of Medicine at University of California Los Angeles, Los Angeles, California, USA

²Division of Hematology and Oncology, Department of Medicine, University of California Los Angeles, Los Angeles, California, USA

Abstract

Purpose—The B-cell antigen CD20 provides a target for antibody-based positron emission tomography (immunoPET). We engineered antibody fragments targeting human CD20 and studied their potential as immunoPET tracers in transgenic mice (huCD20TM) and in a murine lymphoma model expressing human CD20.

Experimental Design—Anti-CD20 cys-diabody (cDb) and cys-minibody (cMb) based on rituximab (Rx) and obinutuzumab (GA101) were radioiodinated and used for immunoPET imaging of a murine lymphoma model. Pairwise comparison of obinutuzumab-based antibody fragments labeled with residualizing (⁸⁹Zr) versus non-residualizing (¹²⁴I) radionuclides by region of interest (ROI) analysis of serial PET images was conducted both in the murine lymphoma model and in huCD20TM to assess antigen modulation *in vivo*.

Results—¹²⁴I-GAcDb and ¹²⁴I-GAcMb produced high-contrast immunoPET images of B-cell lymphoma and outperformed the respective rituximab-based tracers. ImmunoPET imaging of huCD20TM showed specific uptake in lymphoid tissues. The use of the radiometal ⁸⁹Zr as alternative label for GAcDb and GAcMb yielded greater target-specific uptake and retention compared with ¹²⁴I-labeled tracers. Pairwise comparison of ⁸⁹Zr- and ¹²⁴I-labeled GAcDb and

Corresponding authors: Kirstin A Zettlitz, Crump Institute for Molecular Imaging, CNSI 4350, 570 Westwood Plaza, Los Angeles, CA 90095-1770. Phone: 310-267-2819; Fax: 310-206-8975; kzettlitz@mednet.ucla.edu. Anna M Wu, Crump Institute for Molecular Imaging, CNSI 4335, 570 Westwood Plaza, Los Angeles, CA 90095-1770. Phone: 310-794-5088; Fax: 310-206-8975; awu@mednet.ucla.edu.

³current address: Regeneron Pharmaceuticals, Inc., 777 Old Saw Mill River Road, Tarrytown, NY 10591, USA

⁴current address: Brigham and Women's Hospital, Medicine/PBB-B4, 75 Francis St, Boston, MA 02115, USA

⁵current address: ImmunGene, Inc., 480 Constitution Ave, Camarillo, CA 93012

Conflict of Interest disclosure statement:

Anna M. Wu is a founder and consultant to ImaginAb, Inc.

All other authors declare no potential conflicts of interest.

Authorship Contributions: K.A.Z., R.T., J.M.T. and A.M.W. designed research; K.A.Z., R.T., S.M.K., and K.K.S. performed research; K.A.Z., R.T., S.M.K., J.M.T. and A.M.W. analyzed data; and K.A.Z. and A.M.W. wrote the paper.

GAcMb allowed assessment of *in vivo* internalization of CD20/antibody complexes and revealed that CD20 internalization differs between malignant and endogenous B cells.

Conclusions—These obinutuzumab-based PET tracers have the ability to noninvasively and quantitatively monitor CD20-expression and have revealed insights into CD20 internalization upon antibody binding *in vivo*. Because they are based on a humanized mAb they have the potential for direct clinical translation and could improve patient selection for targeted therapy, dosimetry prior to radioimmunotherapy (RIT), and prediction of response to therapy.

Keywords

immunoPET; antibody fragments; B-cell lymphoma; Zirconium-89; Iodine-124

Introduction

The CD20 antigen is expressed on the surface of B cells during all stages of B cell development, except early pro-B cells and plasma cells. CD20 expression on B-cell malignancies such as lymphomas and leukemias has proven useful as target for antibody-based diagnosis and therapies. Rituximab was the first anti-CD20 antibody approved by the FDA (1997) for use in oncology and most lymphoma patients now receive rituximab during their treatment as monotherapy or in combination with chemotherapy.(1–3) Rituximab is given to all patients with the same standard dose and scheduling established at licensing (375 mg/m² weekly x 4),(4) regardless of factors known to affect pharmacokinetics and serum levels, such as CD20 expression level and density, tumor burden and localization, number of circulating B lymphocytes and antigen modulation.(5) Although CD20 has long been thought to not shed, internalize or degrade upon antibody binding,(6) several groups describe antigenic modulation, e.g. internalization of Ag/Ab complexes(7,8) and removal of Ag/Ab complexes from the tumor cell by monocytes, a process termed trogocytosis.(9,10) CD20 modulation might contribute to development of resistance to anti-CD20 mAb in B-cell lymphomas.(11–13)

ImmunoPET, as a non-invasive molecular imaging method, combines the target specificity of antibodies with the sensitivity of positron emission tomography (PET).(14,15) Anti-CD20 immunoPET has the potential to enable personalized image-guided therapy by providing crucial information for diagnosis, prognosis, dosing, and evaluation of therapy response in lymphoma patients and could be especially informative as companion diagnostic for subsequent antibody-based therapy. Furthermore, the non-invasive detection of B cells *in vivo* could enable monitoring of immunotherapies, such as reconstitution after B cell depletion, adoptive cell transfers or B cell targeting vaccination and increase the understanding of B cell-mediated disease states (e.g. rheumatoid arthritis, multiple sclerosis, diabetes).(16,17)

Radiolabeled rituximab has successfully been used for PET imaging of human CD20 expressing transgenic mice,(18,19) and both B-cell lymphomas and autoimmune disease in patients.(20,21) However, the long plasma half-life of full length IgGs requires delays between tracer administration and image acquisition in order to achieve sufficient clearance of the radio-antibody and therefore high target-to-background ratios. In contrast, engineered

antibody fragments such as diabodies (scFv dimer) and minibodies (scFv-C_H3) possess pharmacokinetics optimized for imaging. Removal of the constant domains (C_H2, Fc) abolishes effector functions and FcRn-mediated recycling. The reduction of the overall size results in improved tissue penetration and in accelerated blood clearance with half-lives that range from 2 to 5 h for diabodies (renal clearance) and 5–12 h for minibodies (hepatic clearance) in mice.(22)

In this report, we present novel PET imaging agents based on the humanized, type II anti-CD20 mAb obinutuzumab (GA101).(23) Type II anti-CD20 antibodies bind CD20 in a different orientation from type I antibodies (rituximab) and are reported to internalize less rapidly.(7,24) Cell surface retention is preferable for imaging, allowing the use of radioiodinated tracers which show greatly reduced tissue background because iodine can diffuse from the cell upon internalization and degradation of the radioiodinated antibody. As a result we hypothesized that radioiodinated obinutuzumab-based antibody fragments should be superior to rituximab-based fragments for preclinical immunoPET imaging of lymphoma mouse models and ultimately for clinical translation.

To establish the optimal anti-CD20 immunoPET tracer we compared different sized antibody fragments (cys-diabody, 55 kDa and cys-minibody, 80 kDa) based on obinutuzumab (GA101) and Rituximab, radiolabeled with long-lived positron emitters iodine-124 (¹²⁴I, nonresidualizing, t_{1/2} 4.18 days) and zirconium-89 (⁸⁹Zr, residualizing, t_{1/2} 3.27 days). ImmunoPET tracers were evaluated in two preclinical mouse models expressing human CD20. Firstly, in a subcutaneous B-cell lymphoma model (38C13-huCD20) and secondly, in transgenic mice expressing human CD20 on endogenous mature B cells. Furthermore, we utilized the differences regarding uptake and retention of ¹²⁴I- and ⁸⁹Zr-labeled GA101 antibody fragments to assess internalization of CD20/antibody complexes *in vivo* by comparing quantitative PET images over time, revealing differential internalization rates of healthy and malignant B cells.

Methods

Animals and cell lines

The murine B-cell lymphoma line 38C13 expressing human CD20 (38C13-huCD20) was previously described.(25) Both 38C13 and 38C13-huCD20 were cultured in RPMI 1640 (Life Technologies) supplemented with 50 μM 2-mercaptoethanol and 10% FBS.

Protocols for all animal studies were approved by the University of California Los Angeles (UCLA) Animal Research Committee. 6- to 8-week old female SCID mice were purchased from Jackson Laboratory. Allografts were established by injecting 0.5×10⁶ cells in 1:1 medium:Matrigel (BD Bioscience) subcutaneously into the shoulder region and were allowed to grow for 5–8 days. Human CD20 transgenic mice (hCD20TM) have been described previously,(16) and were backcrossed onto BALB/c backgrounds and genotypes confirmed by polymerase chain reaction (PCR).

Generation of ImmunoPET tracers

Cloning, production, purification and radiolabeling of obinutuzumab- and rituximab-based antibody fragments are described in Supplemental Data Methods.

^{124}I -labeled antibody fragments were generated by direct radioiodination (Pierce® Pre-Coated Iodination Tubes, Thermo Scientific). For site-specific ^{89}Zr -radiolabeling, the chelator deferoxamine-maleimide (mal-DFO, Macrocyclics) was conjugated to the reduced C-terminal cysteine of the antibody fragments and radiolabeling was performed as described by Vosjan et al.(26)

ImmunoPET/CT and biodistribution

Approximately 20–25 μg (~1.5 –2.2 MBq) of ^{124}I - or ^{89}Zr -labeled antibody fragments were injected via tail vein into tumor bearing SCID mice or huCD20TM. Thyroid and stomach uptake of radioiodine was blocked with Lugol's iodine and potassium perchlorate, respectively, as previously described.(27) At 4, 8 and 24 h post injection mice were anesthetized using 2% isoflurane and imaged with 10-minute acquisitions on an Inveon microPET scanner, followed by a microCT scan (Siemens). Following microPET/CT imaging, mice were sacrificed and organs and blood were collected, bilateral lymph nodes (mesenteric, inguinal, axil and brachial) were pooled, weighed and gamma counted. The %ID/g was calculated based on a standard containing 1% of the injected dose.

Image Quantitation and Partial-Volume correction

MicroPET images were reconstructed using non-attenuation filtered back-projection (FBP) or maximum a posteriori (MAP) reconstruction. MicroPET/CT overlay images are displayed as whole body maximum intensity projections (MIP). Image analysis was performed using AMIDE.(28)

Tumor uptake values (%ID/g_{ROI}) and volumes were quantified by drawing ellipsoid regions of interest (ROIs) over the entire tumor based on the microCT. The mean voxel value of the microPET scan was converted to %ID/g using the decay-corrected injected dose and empirically determined cylinder factors for ^{124}I and ^{89}Zr , respectively. Partial volume correction was based on the spheric approximation of the tumor volume (ROI) and previously determined recovery coefficient (RC) curves for ^{124}I and ^{89}Zr .(29) Spleen uptake in huCD20TM was quantified by drawing small ellipsoid ROIs (~14 mm³) within the tip of the spleen and %ID/g_{ROI} was calculated without partial volume correction, due to the complexity of organ shape, volume and proximity to organs with high activity (liver, kidneys).

Data Analysis

Data values are reported as mean \pm SD unless indicated otherwise. *Ex vivo* biodistribution values are depicted as box-and-whiskers (min to max) graphs. For statistical analysis paired t tests and one-way ANOVA for comparing 2 or 3 groups, respectively, were performed using GraphPad Prism version 6.00.

Results

Generation of obinutuzumab (GA101) cys-diabody and cys-minibody

The cys-diabody (GAcDb, 54.5 kDa) and cys-minibody (GAcMb, 83.5 kDa) were generated based on the variable domains of obinutuzumab (GA101). Rituximab-based antibody fragments (RxcDb, RxcMb) were generated similarly for comparison. Antibody fragments contain two antigen-binding sites and a C-terminal cysteine for site-specific conjugation (Figures 1A, S1, S2). Purity and correct assembly of purified proteins was confirmed by SDS-PAGE analysis and size-exclusion chromatography (SEC) (Figures 1B, 1C and S1). Engineered antibody fragments retained the antigen binding characteristics of the parental antibodies. GAcDb and GAcMb reached maximal binding at lower levels than rituximab and showed apparent affinities in the low nanomolar range ($K_d \sim 4$ nM, Figure S3).

I-124 immunoPET and biodistribution in mice bearing subcutaneous B-cell lymphomas

Anti-CD20 cDb and cMb were successfully radiolabeled with ^{124}I or ^{89}Zr (results are summarized in Table 1). Radiochemical purity after size exclusion spin column was >98% for all tracers. Immunoreactivity of radiolabeled antibody fragments ranged from 65–85% (Figure S4).

In vivo targeting of the antibody fragments was evaluated in SCID mice bearing subcutaneous lymphoma tumors (38C13-huCD20). Mice received 20–25 μg (1.5–2.2 MBq) of labeled protein i.v. and were serially imaged at 4, 8 and 24 h p.i. Figure 2 displays representative time series of PET/CT scans showing specific uptake in huCD20-positive tumors and fast clearance from blood and nonspecific tissues, resulting in high-contrast immunoPET images as early as 4 hours p.i.. Background activity cleared by 24 h p.i. with only antigen-positive tumors visible in the PET scan. Specificity of tumor uptake was confirmed in mice bearing 38C13-huCD20 tumors that were blocked by co-injection of 80 μg (4 mg/kg) cold antibody fragments and in mice bearing huCD20-negative 38C13 tumors. The comparison of ^{124}I -GAcDb and ^{124}I -RxcDb (Figure 2A,B) showed that ^{124}I -RxcDb cleared more quickly from the blood as indicated by decreasing activity in the heart and lower uptake in antigen-positive tumors. These observations were confirmed by *ex vivo* biodistribution at 24 h p.i. (Figure 2B, Table S1). Uptake of ^{124}I -GAcDb in 38C13-huCD20 tumors was 4.6 ± 0.6 %ID/g at 24 h p.i. and was significantly higher than in 38C13 control tumors (0.5 ± 0.1 %ID/g, $p < .0001$). ^{124}I -RxcDb showed 1.8 ± 0.4 %ID/g uptake in 38C13-huCD20 tumors and 0.8 ± 0.1 %ID/g in 38C13 ($p < .0001$).

ImmunoPET with ^{124}I -labeled GAcMb (Figure 2C) showed higher activity in the blood (heart), likely due to the longer plasma half-life of the 80 kDa antibody fragment, resulting in higher tumor uptake compared with ^{124}I -GAcDb. Uptake values as determined by *ex vivo* biodistribution (Figure 2D, Table S1) were 9.2 ± 0.8 %ID/g in the 38C13-huCD20 tumors. Uptake in blocked tumors and in CD20-negative 38C13 tumors was significantly lower (3.8 ± 0.3 %ID/g, $p = .0004$ and 1.9 ± 0.3 %ID/g, $p < .0001$, respectively). ^{124}I -RxcMb immunoPET (Figure 2D) also showed tracer uptake in the positive tumors (1.2 ± 0.1 %ID/g), which could be blocked by co-injection of cold RxcMb (0.6 ± 0.2 %ID/g) and

was not observed in negative tumors (0.45 ± 0.2 %IF/g). 38C13-huCD20 uptake values of ^{124}I -RxcMb were considerably lower compared with ^{124}I -GAcMb.

In summary, ^{124}I -GAcDb and ^{124}I -GAcMb outperformed the respective rituximab-based tracers (^{124}I -RxcDb and ^{124}I -RxcMb) reaching higher tumor uptake and higher contrast microPET images (higher target-to-blood ratio). Furthermore, while ^{124}I -GAcMb reached the highest tumor uptake, the faster clearing ^{124}I -GAcDb reached the highest tumor-to-blood ratio at 24 h p.i. (12.4 ± 2.5 , Table S1), resulting in better image contrast.

Zr-89 ImmunopET and biodistribution in mice bearing subcutaneous B-cell lymphomas

To investigate if a residualizing radiometal (^{89}Zr) may be advantageous in terms of greater tumor uptake and retention, mal-DFO was site-specifically conjugated to GAcDb and GAcMb for ^{89}Zr immunopET. Both ^{89}Zr -GAcDb and ^{89}Zr -GAcMb were used for serial immunopET imaging of the 38C13-huCD20 lymphoma model and high-contrast images showing specific tumor uptake were obtained (Figure 3). The residualizing nature of the ^{89}Zr radio-metabolites caused higher nonspecific uptake, especially in organs of clearance (kidneys, liver and spleen) (Figure 3A,B, Table S1). Compared to the respective iodinated cys-diabody, ^{89}Zr -GAcDb reached only slightly higher tumor uptake (4.9 ± 0.3 %ID/g by *ex vivo* biodistribution) resulting in comparable tumor-to-blood ratios while the tumor-to-background (muscle) ratio was lower. ^{89}Zr -GAcDb immunopET images confirmed primarily renal clearance of the 55 kDa protein.

^{89}Zr -GAcMb immunopET showed the highest uptake of all tested tracers in 38C13-huCD20 allogeneic grafts (21.8 ± 1.2 %ID/g) and primarily hepatic clearance. Blood activities were comparable to ^{124}I -GAcMb, resulting in a higher tumor-to-blood ratio for ^{89}Zr -GAcMb (11.0 ± 1.0) compared with ^{124}I -GAcMb (4.0 ± 0.5 , Table S1). However, the tumor-to-muscle ratio was lower (41.1 ± 2.8 and 145.4 ± 19.3 , respectively) caused by higher background retention of the residualizing ^{89}Zr radio-metabolites.

I-124 and Zr-89 ImmunopET of the normal B-cell compartment in huCD20 transgenic mice

To evaluate the *in vivo* targeting ability of the obinutuzumab-based PET tracers in the context of normal tissue expression of CD20, a transgenic mouse model expressing human CD20 (huCD20TM) was used. (16) PET/CT images of mice injected with ^{124}I - and ^{89}Zr -labeled GAcDb and GAcMb were obtained 4, 8 and 20 hours p.i.. All tracers showed rapid and specific localization to the spleen and lymph nodes, where B cells reside (Figure 4A,B and Figure S5). Specificity was confirmed in antigen negative BALB/c mice (Table S2)

The activity in the spleen decreased considerably more quickly with ^{124}I -labeled cDb and cMb compared with ^{89}Zr -labeled cDb and cMb. The mean spleen uptake values (%ID/g \pm SEM) determined by *ex vivo* biodistribution at 20 h p.i. were 5.0 ± 0.4 for ^{124}I -GAcDb compared to 17.8 ± 2.4 for ^{89}Zr -GAcDb ($p = .006$) and 11.5 ± 1.2 for ^{124}I -GAcMb compared to 38.9 ± 5.7 for ^{89}Zr -GAcMb ($p = .003$) (Figure 4C,D and Table S2). Due to the partial volume effect, small structures such as lymph nodes were difficult to visualize, especially with the radioiodinated antibody fragments, although *ex vivo* biodistribution confirmed tracer uptake in dissected lymph nodes (inguinal, axillary, mesenteric) to be 3.0 ± 1.0 %ID/g for ^{124}I -GAcDb and 7.1 ± 0.3 %ID/g for ^{124}I -GAcMb. Here, the use of

residualizing ^{89}Zr -labeled anti-CD20 antibody fragments was advantageous and resulted in clearly distinguishable lymph nodes (Figure S5, microPET 2 mm section, rescaled).

***In vivo* internalization of CD20/antibody complexes from malignant and endogenous B cells**

Pairwise evaluation of both ^{124}I - and ^{89}Zr -labeled antibody fragments over time provides an assessment of *in vivo* binding and internalization of the antigen/antibody complexes.(30) The ^{124}I -labeled antibody fragments undergo intracellular catabolism and dehalogenation upon internalization and ^{124}I -iodotyrosine diffuses rapidly from the cell. ^{89}Zr -antibody fragments show identical target cell binding but noticeable differences in retention because the residualizing ^{89}Zr radio-metabolites are trapped intracellularly.(31)

ImmunoPET studies showed that both ^{124}I - and ^{89}Zr -anti-CD20 tracers result in high-contrast imaging, but differences were observed in uptake and retention of activity in the spleen of huCD20TM compared with the subcutaneous B-cell lymphoma model, suggesting differences in CD20 internalization or modulation between healthy B cells and B-cell lymphomas. Therefore, region of interest (ROI) quantification of serial microPET images and comparison of the change in radioactive signal was performed for ^{124}I - and ^{89}Zr -labeled GA101 antibody fragments in both the s.c. 38C13-huCD20 tumors and in huCD20TM. Peak uptake of the GAcMb appeared around 4–8 h post injection, whereas the smaller GAcDb reached peak uptake before the 4 h time point (Figure 5A). For both antibody fragments the ^{89}Zr -labeled and ^{124}I -labeled versions showed similar uptake and retention in s.c. tumors, indicating no or very slow internalization of the radiotracers within 24 h p.i.

Spleen uptake values in huCD20TM from ^{124}I -labeled GAcDb and GAcMb decreased rapidly from the spleen, at a rate faster than that in the subcutaneous lymphoma model. In contrast, activity from ^{89}Zr -labeled GAcDb and GAcMb was retained in the spleen, resulting in significantly different ROI values for the respective GAcDb ($p=0.0007$) and GAcMb ($p=0.0003$) tracers 24 h p.i. (Figure 5B). This observation indicates that endogenous B cells in the spleen internalize CD20/antibody complexes more rapidly than the B-cell lymphoma 38C13.

Discussion

In this study, we evaluated two obinutuzumab (GA101)-based antibody fragments (cys-diabody, GAcDb and cys-minibody, GAcMb) for immunoPET of CD20 expressing B cells using two alternative radiolabels (^{89}Zr and ^{124}I). To ensure a biologically inert imaging agent, the reformatted antibody fragments lack a full Fc region reducing the interaction with complement or FcRs.(32–34) Both the cDb and the cMb retained binding characteristics (type II epitope and apparent affinity $K_D \sim 4$ nM) of the parental mAb.(23) Because the antibody fragments are based on a humanized mAb, translation into the clinic is facilitated.

Independent of the radiolabeling method (random iodination of tyrosine residues or site-specific conjugation of maleimide-DFO ^{89}Zr to the reduced cys-tag) GA101-based fragments showed specific targeting to human CD20 expressing B cells as demonstrated in a subcutaneous B-cell lymphoma model (38C13-huCD20) and in a transgenic mouse model

expressing human CD20 (huCD20TM). Rapid clearance of the antibody fragments enabled high-contrast small animal PET imaging at early time points.

In the lymphoma model, the ^{124}I -labeled GA101 cDb and cMb outperformed the respective rituximab-based antibody fragments, reaching higher tumor activity (4.6 vs 1.8 %ID/g for cDbs and 9.2 vs 1.2 %ID/g for cMbs at 24 h p.i., respectively) and higher tumor-to-blood ratios. This finding was unexpected considering that type II mAbs (obinutuzumab, GA101) show binding at approximately half the surface density of type I binders (rituximab).(24)

The low specific uptake of the rituximab-based fragments is in accordance with previously published anti-CD20 minibody, scFv-Fc and diabody immunoPET imaging of the same lymphoma model.(35,36) Furthermore, rituximab is described to have a faster off-rate than many other anti-CD20 antibodies, which might influence *in vivo* tumor retention.(37,38)

Compared with the ^{124}I -labeled GAcDb and cMb, the ^{89}Zr -labeled antibody fragments achieved slightly higher tumor activity and retention due to the residualizing radiometal, resulting in higher tumor-to-blood ratios at 24 h p.i.; at the same time the tumor-to-background (muscle) ratio is lower caused by increased background activity. As expected, nonspecific uptake is most pronounced in organs of clearance (kidneys, liver, spleen), which in a clinical setting might impede detection of tumors or metastases in those organs. However, by selecting the antibody fragment according to size (diabody or minibody) the elimination pathway can be predetermined. The high uptake of ^{89}Zr -labeled GAcDb and GAcMb in the spleen of SCID mice is most likely caused by the abnormal structure and significantly smaller size (20–35 mg) and was not observed in BALB/c mice.(39)

ImmunoPET of human CD20 transgenic mice (huCD20TM) showed specific tracer uptake in the spleen for both ^{124}I - and ^{89}Zr -labeled GAcDb and GAcMb. Lymph nodes were difficult to visualize with ^{124}I -labeled antibody fragments, although *ex vivo* biodistribution confirmed tracer uptake. Imaging and quantification of small objects such as lymph nodes (approx. 1–3 mm³) is challenging due to their size being near or below the spatial resolution of the Inveon microPET scanner (1.5–1.8 mm) and the increased partial volume effect (PVE) due to a longer mean positron range of ^{124}I compared with ^{89}Zr (3.0 and 1.1 mm, respectively).(29) Another challenge for ^{124}I PET imaging is the simultaneous emission of a 603-keV gamma-ray with about 50% of all positrons (β^+) that falls within the energy window of most PET scanners and causes increased background.(40) ^{89}Zr on the other hand, emits a prompt 909-keV gamma-ray with 100% of positrons but the disparity to the 511 keV photons prevents interference with the detection of coincident photons.(41) Therefore, immunoPET using ^{89}Zr -GAcDb and cMb visualized even small lymph nodes with high contrast.

In summary, for B-cell lymphomas with cell surface retention of Ag/Ab complexes ^{124}I -labeled obinutuzumab antibody fragments outperform rituximab-based fragments and the use of ^{124}I is preferable to ^{89}Zr as it results in higher image contrast due to lower background throughout the organism. On the other hand, for immunoPET imaging of small structures like lymph nodes or metastases and of internalizing antigens the ^{89}Zr -labeled antibody fragments are more suitable.

Recent studies in a similar transgenic mouse model using ^{89}Zr -labeled intact rituximab showed high uptake in the spleen (103 ± 12 %ID/g at 24 h p.i. from *ex vivo* biodistribution) but no uptake in lymph nodes.(19) Possible explanations include the low injected protein dose (2–3 μg) resulting in rapid accumulation of the tracer in the spleen. The abundance of CD20 antigen throughout the body and high concentration of antigen in the spleen (antigen sink) makes imaging outside the sink challenging. In contrast to the antibody fragments presented in our study, the radiolabeled intact rituximab is biologically active and would deplete B cells if injected at higher doses. The ability of the obinutuzumab-based tracers to image small structures (lymph nodes) outside the antigen sink at low doses (15–20 μg protein/dose) will be crucial for imaging in the context of normal tissue distribution of CD20.

Muylle et al. investigated the impact of preloading with unlabeled rituximab on tumor targeting using ^{89}Zr -rituximab immunoPET in lymphoma patients and found impaired tumor targeting in the majority of patients.(21) This study showed that tumor targeting is influenced by a variety of factors, e.g. B-cell depletion, spleen volume, tumor heterogeneity, the site of tumor involvement and preload of unlabeled antibody. The authors emphasize the potential of immunoPET as an inherently quantitative imaging method, for dosimetry prior to radioimmunotherapy (RIT), better selection of patients for targeted therapy and prediction of treatment outcome.

Dosimetry studies with ^{89}Zr -labeled full-length antibodies in patients have suggested that nonspecific accumulation in the liver will be dose limiting, while for ^{124}I -labeled tracers bone marrow exposure from blood activity is usually the limiting factor.(42–44) A dosimetry study based on biodistribution data of ^{89}Zr -rituximab in huCD20TM suggest liver (with pre-dose) and spleen (without pre-dose) as dose-limiting organs in humans.(45) In both cases, the use of a smaller, fast-clearing antibody fragment like the cys-diabody and the cys-minibody could result in a reduction of the radiation exposure and absorbed dose to the patient.

In addition to confirming presence of target antigen *in vivo*, immunoPET has also been used to evaluate antigen modulation by pairwise comparison of residualizing and non-residualizing radiolabels conjugated to the same antibody. This was demonstrated for the slow internalization of prostate stem cell antigen (PSCA) bound by ^{124}I -anti-PSCA minibody (^{124}I -A11) and ^{89}Zr -A11;(29) and in a study by Cheal et al. using ^{124}I -cG250 and ^{89}Zr -cG250 to study *in vivo* receptor binding and internalization of carbonic anhydrase IX. (30) In the present study, serial ROI analysis of ^{124}I -GAcDb and ^{124}I -GAcMb immunoPET in huCD20TM showed that radioactivity decreased significantly faster from the spleen compared with the retention of activity using ^{89}Zr -GAcDb and ^{89}Zr -GAcMb. In contrast, the radioiodinated and radiometal labeled tracers demonstrated very similar retention in the subcutaneous lymphoma tumors. This suggests that CD20/GA101 complexes are indeed internalized and metabolized rapidly in huCD20 Tg B cells, compared to slower internalization in 38C13-huCD20 lymphoma cells. The results of our study are consistent with previous *in vitro* observations in the literature that tissue cultured B-cell lines and xenograft models show no significant internalization while primary human B cells and huCD20 Tg B cells show more rapid internalization.(7,8,46) The differences in CD20

internalization seen in these two mouse models don't warrant general conclusions about CD20 modulation in normal and malignant cell line, however, this proof-of-principle study demonstrates the applicability of immunoPET to study the wide heterogeneity in CD20 modulation rates reported for primary lymphomas.

Although the literature regarding CD20 modulation is conflicting, it seems obvious that a substantial reduction of CD20 levels on target B cells and consumption of the therapeutic antibody would impair immunotherapy and might cause resistance. Beers et al. reported rapid CD20 internalization of type I mAb (rituximab) in human CD20Tg B cells,(7) and little modulation of CD20 from the cell surface by type II anti-CD20 mAb (tositumomab). This process appears to be an intrinsic B cell phenomenon that does not require activatory Fc gamma R engagement by effector cells as shown in γ -chain $-/-$ (activatory Fc gamma R-negative) mice. Internalization of CD20/type I mAb complexes occurred equally rapidly (within just 2 hours) in normal human peripheral blood B cells. The same group showed in a recent study that internalization of mAbs is antibody specificity and Fc γ RIIb dependent.(46) Although most bound mAbs bind Fc γ RIIb, internalization of Ag/Ab/FcR complexes occurs only for a select subset (anti-CD20 type I). However, work by Taylor and colleagues (47) demonstrated that an endocytic process, termed trogocytosis, mediated by Fc γ R-expressing effector cells (monocytes, macrophages, or NK cells) might also play a role in promoting CD20/mAb loss *in vivo*. This study showed only modest internalization of rituximab from 38C13-huCD20 cells but substantial removal of CD20 and bound type I mAbs (rituximab and ofatumumab) upon incubation with THP-1 acceptor cells. Consistent with both studies, we found no tracer internalization in subcutaneous 38C13-huCD20 lymphomas but distinct internalization in the spleen (normal B cells) of transgenic mice. Although the rationale for engineering antibody fragments based on a type II anti-CD20 mAb and without the Fc region was to ensure cell surface retention, our findings suggest that a fraction of CD20 internalization is independent of the epitope binding mode and Fc γ RIIb binding.

Future studies should include immunoPET of more physiological relevant models, e.g. syngeneic models of disseminated B-cell lymphoma in immunocompetent mice and imaging of tumors in the context of normal tissue expression in transgenic mice.

In conclusion, we presented novel anti-CD20 antibody fragments that specifically target human CD20 expressed on healthy and malignant B cells and produce high contrast immunoPET images. The combination of antibody fragments (size, plasma half-life, route of clearance) with radionuclides (residualizing vs. non-residualizing) offers optimized tracers for a variety of applications in B cell imaging. The ability to monitor CD20 internalization *in vivo* using noninvasive imaging could have an important impact on understanding B cell biology and support treatment design, especially when immunoPET tracers accompany subsequent antibody based therapies.

Supplementary Material

Refer to Web version on PubMed Central for supplementary material.

Acknowledgments

The authors thank the Preclinical Imaging Technology Center, UCLA Crump Institute for Molecular Imaging for help with small-animal PET scans. Dr. MJ Glennie kindly provided sequence information for the GA101 variable domains. We thank Felix B. Salazar and Reiko E. Yamada for technical assistance. This work was supported by NIH grant CA149254, and by a generous gift from Ralph and Marjorie Crump to the Crump Institute. Small animal imaging and flow cytometry were funded in part by the UCLA Jonsson Comprehensive Cancer Center Support Grant (NIH CA016042).

References

1. Reff ME, Carner K, Chambers KS, Chinn PC, Leonard JE, Raab R, et al. Depletion of B cells in vivo by a chimeric mouse human monoclonal antibody to CD20. *Blood*. 1994; 83(2):435–45. [PubMed: 7506951]
2. Coiffier B, Haioun C, Ketterer N, Engert A, Tilly H, Ma D, et al. Rituximab (anti-CD20 monoclonal antibody) for the treatment of patients with relapsing or refractory aggressive lymphoma: a multicenter phase II study. *Blood*. 1998; 92(6):1927–32. [PubMed: 9731049]
3. Vose JM, Link BK, Grossbard ML, Czuczman M, Grillo-Lopez A, Gilman P, et al. Phase II study of rituximab in combination with chop chemotherapy in patients with previously untreated, aggressive non-Hodgkin's lymphoma. *J Clin Oncol*. 2001; 19(2):389–97. [PubMed: 11208830]
4. Coiffier B, Lepage E, Briere J, Herbrecht R, Tilly H, Bouabdallah R, et al. CHOP chemotherapy plus rituximab compared with CHOP alone in elderly patients with diffuse large-B-cell lymphoma. *N Engl J Med*. 2002; 346(4):235–42. DOI: 10.1056/NEJMoa011795 [PubMed: 11807147]
5. Keizer RJ, Huitema AD, Schellens JH, Beijnen JH. Clinical pharmacokinetics of therapeutic monoclonal antibodies. *Clin Pharmacokinet*. 2010; 49(8):493–507. DOI: 10.2165/11531280-000000000-00000 [PubMed: 20608753]
6. Press OW, Howell-Clark J, Anderson S, Bernstein I. Retention of B-cell-specific monoclonal antibodies by human lymphoma cells. *Blood*. 1994; 83(5):1390–7. [PubMed: 8118040]
7. Beers SA, French RR, Chan HT, Lim SH, Jarrett TC, Vidal RM, et al. Antigenic modulation limits the efficacy of anti-CD20 antibodies: implications for antibody selection. *Blood*. 2010; 115(25): 5191–201. DOI: 10.1182/blood-2010-01-263533 [PubMed: 20223920]
8. Lim SH, Vaughan AT, Ashton-Key M, Williams EL, Dixon SV, Chan HT, et al. Fc gamma receptor IIb on target B cells promotes rituximab internalization and reduces clinical efficacy. *Blood*. 2011; 118(9):2530–40. DOI: 10.1182/blood-2011-01-330357 [PubMed: 21768293]
9. Kennedy AD, Beum PV, Solga MD, DiLillo DJ, Lindorfer MA, Hess CE, et al. Rituximab Infusion Promotes Rapid Complement Depletion and Acute CD20 Loss in Chronic Lymphocytic Leukemia. *The Journal of Immunology*. 2004; 172(5):3280–8. DOI: 10.4049/jimmunol.172.5.3280 [PubMed: 14978136]
10. Williams ME, Densmore JJ, Pawluczko AW, Beum PV, Kennedy AD, Lindorfer MA, et al. Thrice-weekly low-dose rituximab decreases CD20 loss via shaving and promotes enhanced targeting in chronic lymphocytic leukemia. *J Immunol*. 2006; 177(10):7435–43. [PubMed: 17082663]
11. Hiraga J, Tomita A, Sugimoto T, Shimada K, Ito M, Nakamura S, et al. Down-regulation of CD20 expression in B-cell lymphoma cells after treatment with rituximab-containing combination chemotherapies: its prevalence and clinical significance. *Blood*. 2009; 113(20):4885–93. DOI: 10.1182/blood-2008-08-175208 [PubMed: 19246561]
12. Taylor RP, Lindorfer MA. Antigenic modulation and rituximab resistance. *Semin Hematol*. 2010; 47(2):124–32. DOI: 10.1053/j.seminhematol.2010.01.006 [PubMed: 20350659]
13. Tsai PC, Hernandez-Ilizaliturri FJ, Bangia N, Olejniczak SH, Czuczman MS. Regulation of CD20 in rituximab-resistant cell lines and B-cell non-Hodgkin lymphoma. *Clin Cancer Res*. 2012; 18(4): 1039–50. DOI: 10.1158/1078-0432.CCR-11-1429 [PubMed: 22228637]
14. Verel I, Visser GW, van Dongen GA. The promise of immuno-PET in radioimmunotherapy. *J Nucl Med*. 2005; 46(Suppl 1):164S–71S. [PubMed: 15653665]

15. Knowles SM, Wu AM. Advances in immuno-positron emission tomography: antibodies for molecular imaging in oncology. *J Clin Oncol*. 2012; 30(31):3884–92. DOI: 10.1200/JCO.2012.42.4887 [PubMed: 22987087]
16. Ahuja A, Shupe J, Dunn R, Kashgarian M, Kehry MR, Shlomchik MJ. Depletion of B cells in murine lupus: efficacy and resistance. *J Immunol*. 2007; 179(5):3351–61. [PubMed: 17709552]
17. Betting DJ, Kafi K, Abdollahi-Fard A, Hurvitz SA, Timmerman JM. Sulfhydryl-based tumor antigen-carrier protein conjugates stimulate superior antitumor immunity against B cell lymphomas. *J Immunol*. 2008; 181(6):4131–40. [PubMed: 18768870]
18. Natarajan A, Gowrishankar G, Nielsen CH, Wang S, Iagaru A, Goris ML, et al. Positron emission tomography of ⁶⁴Cu-DOTA-Rituximab in a transgenic mouse model expressing human CD20 for clinical translation to image NHL. *Mol Imaging Biol*. 2012; 14(5):608–16. DOI: 10.1007/s11307-011-0537-8 [PubMed: 22231277]
19. Natarajan A, Habte F, Gambhir SS. Development of a novel long-lived immunoPET tracer for monitoring lymphoma therapy in a humanized transgenic mouse model. *Bioconjug Chem*. 2012; 23(6):1221–9. DOI: 10.1021/bc300039r [PubMed: 22621257]
20. Malviya G, Anzola KL, Podesta E, Lagana B, Del Mastro C, Dierckx RA, et al. (99m)Tc-labeled rituximab for imaging B lymphocyte infiltration in inflammatory autoimmune disease patients. *Mol Imaging Biol*. 2012; 14(5):637–46. DOI: 10.1007/s11307-011-0527-x [PubMed: 22127469]
21. Muylle K, Flamen P, Vugts DJ, Guiot T, Ghanem G, Meuleman N, et al. Tumour targeting and radiation dose of radioimmunotherapy with (90)Y-rituximab in CD20+ B-cell lymphoma as predicted by (89)Zr-rituximab immuno-PET: impact of preloading with unlabelled rituximab. *Eur J Nucl Med Mol Imaging*. 2015; 42(8):1304–14. DOI: 10.1007/s00259-015-3025-6 [PubMed: 25792453]
22. Olafsen T, Wu AM. Antibody vectors for imaging. *Semin Nucl Med*. 2010; 40(3):167–81. DOI: 10.1053/j.semnucmed.2009.12.005 [PubMed: 20350626]
23. Mossner E, Bruncker P, Moser S, Puntener U, Schmidt C, Herter S, et al. Increasing the efficacy of CD20 antibody therapy through the engineering of a new type II anti-CD20 antibody with enhanced direct and immune effector cell-mediated B-cell cytotoxicity. *Blood*. 2010; 115(22):4393–402. DOI: 10.1182/blood-2009-06-225979 [PubMed: 20194898]
24. Beers SA, Chan CH, James S, French RR, Attfield KE, Brennan CM, et al. Type II (tositumomab) anti-CD20 monoclonal antibody out performs type I (rituximab-like) reagents in B-cell depletion regardless of complement activation. *Blood*. 2008; 112(10):4170–7. DOI: 10.1182/blood-2008-04-149161 [PubMed: 18583569]
25. Betting DJ, Yamada RE, Kafi K, Said J, van Rooijen N, Timmerman JM. Intratumoral but not systemic delivery of CpG oligodeoxynucleotide augments the efficacy of anti-CD20 monoclonal antibody therapy against B cell lymphoma. *J Immunother*. 2009; 32(6):622–31. DOI: 10.1097/CJI.0b013e3181ab23f1 [PubMed: 19483647]
26. Vosjan MJ, Perk LR, Visser GW, Budde M, Jurek P, Kiefer GE, et al. Conjugation and radiolabeling of monoclonal antibodies with zirconium-89 for PET imaging using the bifunctional chelate p-isothiocyanatobenzyl-desferrioxamine. *Nat Protoc*. 2010; 5(4):739–43. DOI: 10.1038/nprot.2010.13 [PubMed: 20360768]
27. Lepin EJ, Leyton JV, Zhou Y, Olafsen T, Salazar FB, McCabe KE, et al. An affinity matured minibody for PET imaging of prostate stem cell antigen (PSCA)-expressing tumors. *Eur J Nucl Med Mol Imaging*. 2010; 37(8):1529–38. DOI: 10.1007/s00259-010-1433-1 [PubMed: 20354850]
28. Loening AM, Gambhir SS. AMIDE: a free software tool for multimodality medical image analysis. *Mol Imaging*. 2003; 2(3):131–7. [PubMed: 14649056]
29. Knowles SM, Zettlitz KA, Tavare R, Rochefort MM, Salazar FB, Stout DB, et al. Quantitative immunoPET of prostate cancer xenografts with ⁸⁹Zr- and ¹²⁴I-labeled anti-PSCA A11 minibody. *J Nucl Med*. 2014; 55(3):452–9. DOI: 10.2967/jnumed.113.120873 [PubMed: 24504052]
30. Cheal SM, Punzalan B, Doran MG, Evans MJ, Osborne JR, Lewis JS, et al. Pairwise comparison of ⁸⁹Zr- and ¹²⁴I-labeled cG250 based on positron emission tomography imaging and nonlinear immunokinetic modeling: in vivo carbonic anhydrase IX receptor binding and internalization in mouse xenografts of clear-cell renal cell carcinoma. *Eur J Nucl Med Mol Imaging*. 2014; 41(5):985–94. DOI: 10.1007/s00259-013-2679-1 [PubMed: 24604591]

31. van Dongen GA, Visser GW, Lub-de Hooge MN, de Vries EG, Perk LR. Immuno-PET: a navigator in monoclonal antibody development and applications. *Oncologist*. 2007; 12(12):1379–89. DOI: 10.1634/theoncologist.12-12-1379 [PubMed: 18165614]
32. Brekke OHMT, Sandlie I. The structural requirements for complement activation by IgG, does it hinge on the hinge. *Immunology Today*. 1995
33. Wines BD, Powell MS, Parren PW, Barnes N, Hogarth PM. The IgG Fc contains distinct Fc receptor (FcR) binding sites: the leukocyte receptors Fc gamma RI and Fc gamma RIIa bind to a region in the Fc distinct from that recognized by neonatal FcR and protein A. *J Immunol*. 2000; 164(10):5313–8. [PubMed: 10799893]
34. Vidarsson G, Dekkers G, Rispens T. IgG subclasses and allotypes: from structure to effector functions. *Front Immunol*. 2014; 5:520.doi: 10.3389/fimmu.2014.00520 [PubMed: 25368619]
35. Olafsen T, Betting D, Kenanova VE, Salazar FB, Clarke P, Said J, et al. Recombinant anti-CD20 antibody fragments for small-animal PET imaging of B-cell lymphomas. *J Nucl Med*. 2009; 50(9): 1500–8. DOI: 10.2967/jnumed.108.060426 [PubMed: 19690034]
36. Olafsen T, Sirk SJ, Betting DJ, Kenanova VE, Bauer KB, Ladno W, et al. ImmunoPET imaging of B-cell lymphoma using 124I-anti-CD20 scFv dimers (diabodies). *Protein Eng Des Sel*. 2010; 23(4):243–9. DOI: 10.1093/protein/gzp081 [PubMed: 20053640]
37. Teeling JL, Mackus WJ, Wiegman LJ, van den Brakel JH, Beers SA, French RR, et al. The biological activity of human CD20 monoclonal antibodies is linked to unique epitopes on CD20. *J Immunol*. 2006; 177(1):362–71. [PubMed: 16785532]
38. Goldenberg DM, Rossi EA, Stein R, Cardillo TM, Czuczman MS, Hernandez-Ilizaliturri FJ, et al. Properties and structure-function relationships of veltuzumab (hA20), a humanized anti-CD20 monoclonal antibody. *Blood*. 2009; 113(5):1062–70. DOI: 10.1182/blood-2008-07-168146 [PubMed: 18941114]
39. Economopoulos V, Noad JC, Krishnamoorthy S, Rutt BK, Foster PJ. Comparing the MRI appearance of the lymph nodes and spleen in wild-type and immuno-deficient mouse strains. *PLoS One*. 2011; 6(11):e27508.doi: 10.1371/journal.pone.0027508 [PubMed: 22096586]
40. Lubberink M, Herzog H. Quantitative imaging of 124I and 86Y with PET. *Eur J Nucl Med Mol Imaging*. 2011; 38(Suppl 1):S10–8. DOI: 10.1007/s00259-011-1768-2 [PubMed: 21484385]
41. Deri MA, Zeglis BM, Francesconi LC, Lewis JS. PET imaging with (8)(9)Zr: from radiochemistry to the clinic. *Nucl Med Biol*. 2013; 40(1):3–14. DOI: 10.1016/j.nucmedbio.2012.08.004 [PubMed: 22998840]
42. Borjesson PK, Jauw YW, de Bree R, Roos JC, Castelijns JA, Leemans CR, et al. Radiation dosimetry of 89Zr-labeled chimeric monoclonal antibody U36 as used for immuno-PET in head and neck cancer patients. *J Nucl Med*. 2009; 50(11):1828–36. DOI: 10.2967/jnumed.109.065862 [PubMed: 19837762]
43. Holland JP, Divilov V, Bander NH, Smith-Jones PM, Larson SM, Lewis JS. 89Zr-DFO-J591 for immunoPET of prostate-specific membrane antigen expression in vivo. *J Nucl Med*. 2010; 51(8): 1293–300. DOI: 10.2967/jnumed.110.076174 [PubMed: 20660376]
44. Schwartz J, Humm JL, Divgi CR, Larson SM, O'Donoghue JA. Bone marrow dosimetry using 124I-PET. *J Nucl Med*. 2012; 53(4):615–21. DOI: 10.2967/jnumed.111.096453 [PubMed: 22414633]
45. Natarajan A, Gambhir SS. Radiation Dosimetry Study of [(89)Zr]rituximab Tracer for Clinical Translation of B cell NHL Imaging using Positron Emission Tomography. *Mol Imaging Biol*. 2015; 17(4):539–47. DOI: 10.1007/s11307-014-0810-8 [PubMed: 25500766]
46. Vaughan AT, Iriyama C, Beers SA, Chan CH, Lim SH, Williams EL, et al. Inhibitory FcγRIIb (CD32b) becomes activated by therapeutic mAb in both cis and trans and drives internalization according to antibody specificity. *Blood*. 2014; 123(5):669–77. DOI: 10.1182/blood-2013-04-490821 [PubMed: 24227819]
47. Beum PV, Peek EM, Lindorfer MA, Beurskens FJ, Engelberts PJ, Parren PW, et al. Loss of CD20 and bound CD20 antibody from opsonized B cells occurs more rapidly because of trogocytosis mediated by Fc receptor-expressing effector cells than direct internalization by the B cells. *J Immunol*. 2011; 187(6):3438–47. DOI: 10.4049/jimmunol.1101189 [PubMed: 21841127]

Statement of translational relevance

Diagnostic imaging for staging and response monitoring (FDG PET/CT) in lymphoma patients does not provide direct information about the prominent therapy target CD20. Immuno-positron emission tomography (immunoPET) represents a non-invasive approach to assess in vivo target expression and distribution. In this work, we evaluate novel antibody fragments targeting human CD20 and demonstrate high-contrast immunoPET imaging of human CD20-expressing murine lymphoma and of the normal B-cell compartment in transgenic mice. Pairwise comparison of ^{89}Zr - and ^{124}I -labeled antibody fragments by serial PET imaging allowed assessment of internalization of the radioantibody in vivo. These obinutuzumab-based PET tracers have the potential for direct clinical translation and could provide useful information for diagnosis, therapy selection, dosing or response to therapy.

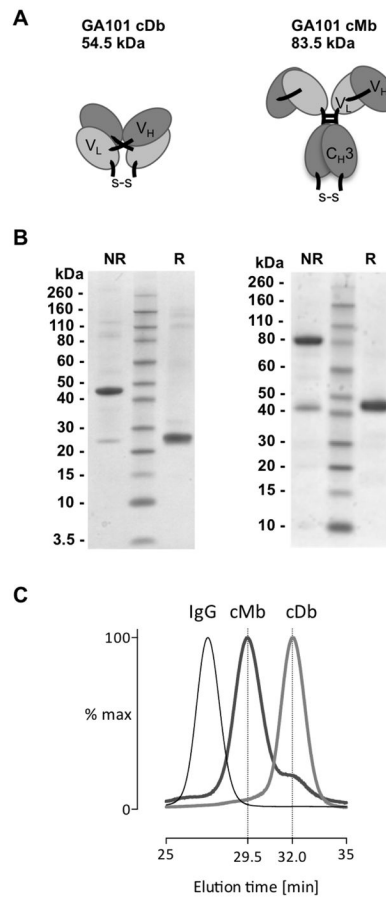


Figure 1. Production and Characterization of engineered obinutuzumab (GA101) antibody fragments

(A) Schematic representation of cys-diabody and cys-minibody antibody fragments. The heavy and light chain variable regions of obinutuzumab (GA101) are connected by glycine-rich linkers of 5 amino acid (G_4S , diabody) and 15 amino acids ($(G_4S)_3$, minibody) length, respectively. Downstream of the V_H domain the human gamma 1 hinge and C_H3 domain were inserted to form the minibody. Both antibody fragments contain a C-terminal histidine-cysteine tag (H_6 -GGC). (B) SDS-PAGE analysis of purified GA101 cys-diabody and cys-minibody under non-reducing (NR) and reducing (R) conditions. (C) Size exclusion chromatography of the engineered GA101 antibody fragments in comparison to full length IgG.

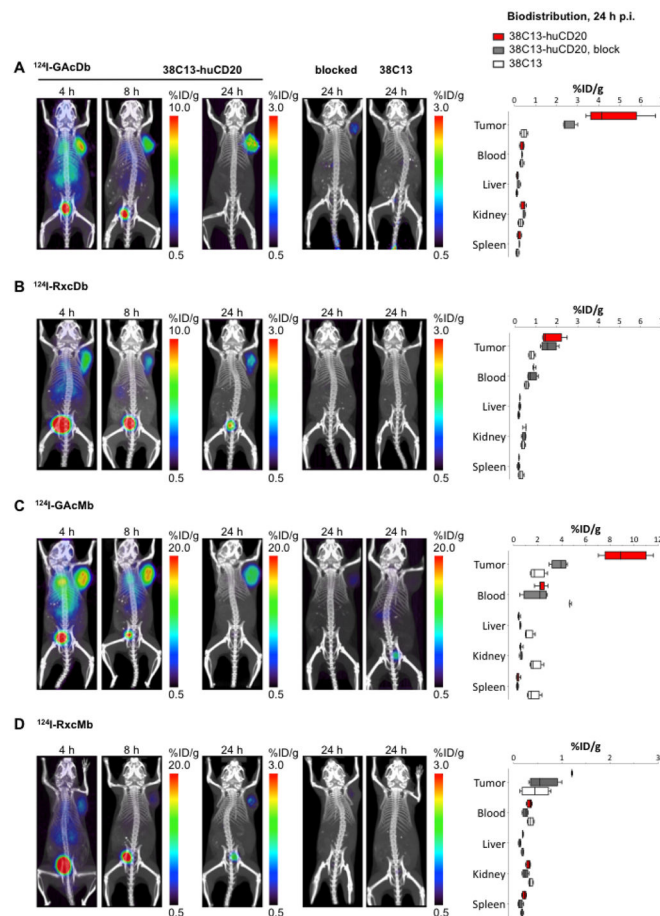


Figure 2. ^{124}I -obinutuzumab (GA101)-based antibody fragments outperform ^{124}I -rituximab-based antibody fragments for *in vivo* immunopET imaging of subcutaneous B-cell lymphoma Representative serial immunopET images of mice bearing s.c. 38C13-huCD20 tumors, blocked (bolus injection of cold antibody fragment), or CD20-negative 38C13 tumors at 4, 8 and 24 hours post injection of 20–25 μg of ^{124}I -labeled antibody fragments. All anti-CD20 tracers show *in vivo* specificity to the CD20-expressing B-cell lymphoma. (A) ^{124}I -GA cDb, (B) ^{124}I -Rx cDb. (C) ^{124}I -GA cMb. (D) ^{124}I -Rx cMb. Small-animal PET images (FBP reconstruction) are shown as full body maximum intensity projection overlaid with microCT. After the last microPET scan mice were sacrificed and *ex vivo* biodistribution performed (24 h p.i., n = 4). %ID/g values of each group are depicted as box-and-whisker plot (min-max).

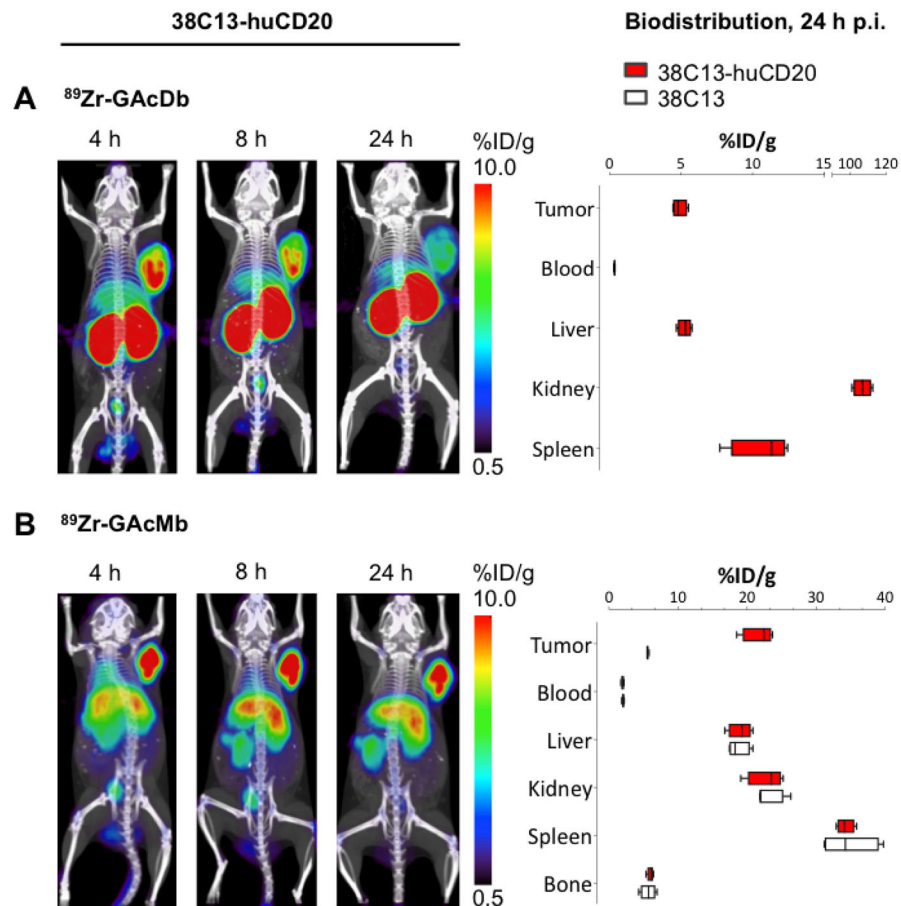


Figure 3. ⁸⁹Zr-labeled obinutuzumab-based antibody fragments for *in vivo* immunoPET imaging of subcutaneous B-cell lymphoma

(A) ⁸⁹Zr-GA101 cys-diabody and (B) ⁸⁹Zr-GA101 cys-minibody immunoPET in mice bearing s.c. 38C13-huCD20 tumors (right shoulder) showed specific uptake in the tumor and distinct routes of clearance (renal for cys-diabody and hepatic for cys-minibody, respectively). Small-animal PET images (FBP reconstruction) are shown as full body maximum intensity projection overlaid with microCT. *Ex vivo* biodistribution (24 h p.i., n 4) were performed for of each group (38C13-huCD20 and 38C13). %ID/g values are depicted as box-and-whisker plot (min-max).

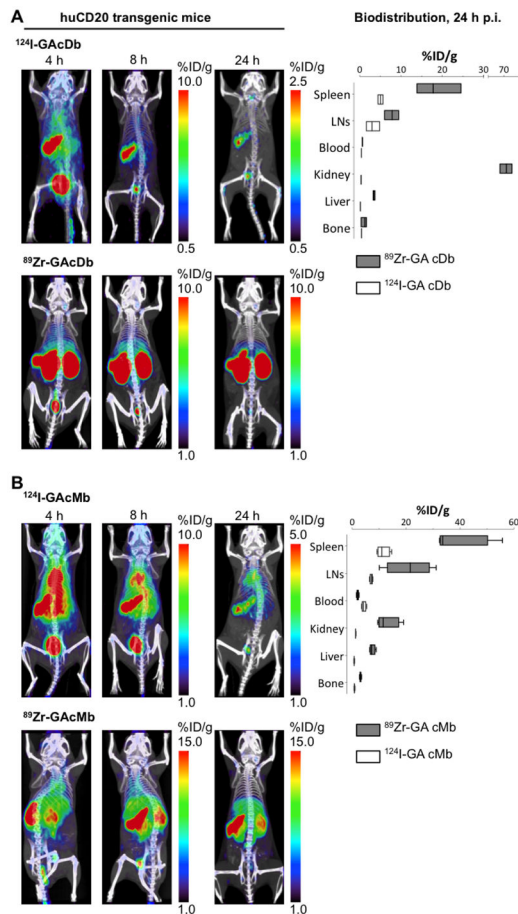


Figure 4. *In vivo* immunopET imaging of the B-cell compartment in huCD20TM (A) ^{124}I - and ^{89}Zr -GA101 cys-diabody (GAcDb) and (B) ^{124}I - and ^{89}Zr -GA101 cys-minibody (GAcMb) immunoPET in transgenic mice expressing human CD20 on mature B cells showed specific uptake in the spleen and lymph nodes. GAcDb showed high contrast images at earlier time points and renal clearance while GAcMb showed higher uptake in target organs and mainly hepatic clearance. Small-animal PET images (MAP reconstructions) are shown as full body maximum intensity projection overlaid with microCT. *Ex vivo* biodistribution 24 h p.i., n = 3. %ID/g values of each group (^{124}I and ^{89}Zr -labeled) are depicted as box-and-whisker plot (min-max).

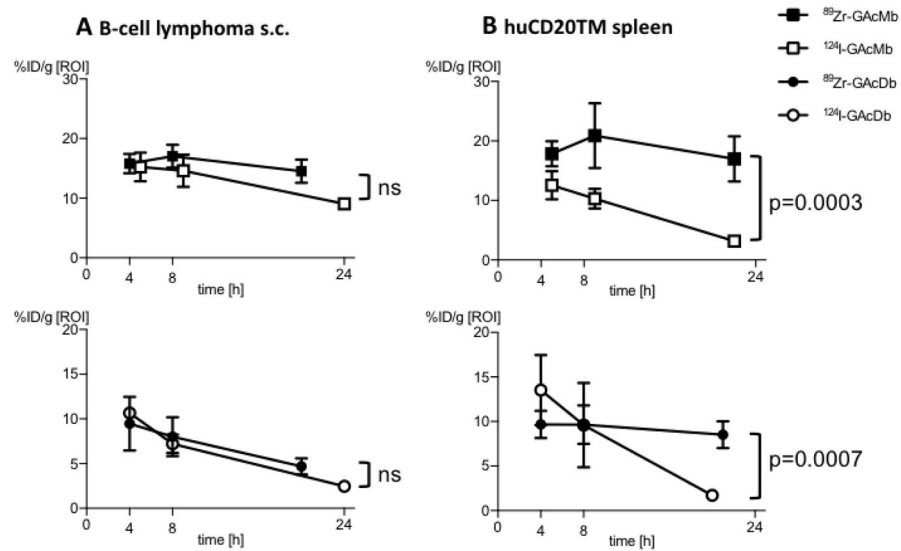


Figure 5. Assessment of *in vivo* CD20/antibody fragment internalization using quantitative ROI analysis

Quantification of regions of interest (ROI) of serial immuno-PET images with ^{124}I - and ^{89}Zr -labeled GA101 antibody fragments. Elliptic ROIs were drawn over the entire tumor or the tip of the spleen, respectively. (A) Partial volume corrected tumor uptake values (%ID/g ROI) from PET images acquired 4, 8 and 24 h p.i. showed similar clearance from human CD20 expressing 38C13 s.c. tumors indicating that internalization did not occur. (B) ROI analysis of tracer uptake in the spleen of transgenic mice expressing huCD20 revealed fast clearance of ^{124}I -labeled fragments while ^{89}Zr -labeled antibody fragments showed retained activity indicating that naïve B cells internalize CD20-antibody complexes. Values are represented as mean \pm SD; * $P < 0.05$; **** $P < 0.0001$, ns = not significant.

Radiolabeling of engineered antibody fragments. Labeling efficiency (LE), radiochemical purity (RCP) and specific activity (SA). Data are presented as mean \pm SD.

Table 1

	^{125}I -GAcDb	^{89}Zr -GAcDb	^{125}I -GAcMb	^{89}Zr -GAcMb	^{125}I -RxcMb	^{89}Zr -RxcMb
LE [%]	70.2 \pm 20.2	85.2 \pm 10.4	63.0 \pm 19.8	95.3 \pm 2.6	80.4 \pm 2.8	76.5 \pm 8.9
RCP [%]	99.4 \pm 0.3	97.7 \pm 1.6	98.7 \pm 1.5	98.4 \pm 1.5	98.1 \pm 0.4	99.2 \pm 0.3
SA [$\mu\text{Ci}/\mu\text{g}$]	2.4 \pm 1.1	2.7 \pm 1.3	3.0 \pm 2.5	3.2 \pm 0.7	1.8 \pm 0.2	3.8 \pm 0.1
SA [MBq/mg]	89.5 \pm 41.4	101 \pm 48	113 \pm 92	117 \pm 27	66.6 \pm 6.3	141 \pm 4
N	10	3	6	3	3	4